

## Nanocomposite of modified montmorillonite K10 with $\text{SiO}_2\text{-Fe}_2\text{O}_3$ as a catalyst of biodiesel synthesis

Serly Jolanda Sekewael<sup>1\*</sup>, Karna Wijaya<sup>2</sup>, Triyono<sup>2</sup>, Arief Budiman<sup>3</sup>

<sup>1\*</sup>Department of Chemistry, FMIPA, Pattimura University, Ambon, Indonesia

<sup>2</sup>Department of Chemistry, FMIPA, GadjahMada University, Yogyakarta, Indonesia

<sup>3</sup>Department of Chemical Engineering, Faculty of Engineering, GadjahMada University, Yogyakarta, Indonesia

**Abstract :** Chemically modified montmorillonite K10 (Mt-K10) with a mixture of  $\text{SiO}_2\text{-Fe}_2\text{O}_3$  oxide was done through the intercalation of silica-iron sol into the interlayer of montmorillonite followed by calcination using microwave radiation 700 W for 10 minutes. Characterization of physical and chemical properties of the reaction product (nanocomposite SFMK-700) and Mt-K10 using XRD, FTIR, BET surface area analyzer (porosimetry), TEM, and SEM-EDAX instruments. Total surface acidity has also been tested. The results showed that the physicochemical modified of Mt-K10 resulted in increased acidity and catalyst activity. The catalyst activity test carried out on lauric acid esterification with methanol (molar ratio of 1:20) in the presence of a 20% (w/w) catalyst. The catalyst SFMK-700 is capable of converting 95.92% lauric acid to form a product of methyl laurate (methyl ester/biodiesel) as much as 93.74% (w/w).

**Key words :** montmorillonite K10,  $\text{SiO}_2\text{-Fe}_2\text{O}_3$ , catalyst of biodiesel synthesis.

### 1. Introduction

The use of montmorillonite K10 (Mt-K10) and its modified structure as solid acid catalysts in various organic reactions have been carried out by several researchers<sup>1,2,3,4</sup>. The catalysts are known to potentially as solid acid catalysts: environmentally friendly, non-corrosive, working at intermediate temperatures, and has the potential to replace conventional acid catalyst to the conversion of reactants into a great product.

A new procedure for the synthesis of modified Mt-K10 with mixed oxide  $\text{SiO}_2\text{-ZrO}_2$  was proposed in our previous study<sup>5</sup>. In this work, mixed oxide  $\text{SiO}_2\text{-Fe}_2\text{O}_3$  was used to modified the Mt-K10 resulted a synthesized nanocomposite to investigate its activity as a catalyst for the synthesis of methyl ester (biodiesel). For this purpose, mixed oxide  $\text{SiO}_2\text{-Fe}_2\text{O}_3$  was prepared *via* sol-gel process. Positively charged metal oxide sols of  $\text{SiO}_2\text{-Fe}_x(\text{OH})_y$  may be intercalated into the interlayer of Mt-K10 by cation-exchange reactions, providing modified materials after calcination. The physicochemical properties were systematically investigated by XRD, gas sorption analyzer, FTIR, TEM, SEM-EDAX, along with a preliminary test on catalytic activity for the lauric acid esterification.

## 2. Research Method

### 2.1 Chemicals and instruments

#### Chemicals:

Mt-K10 (Fluka, Chemica), aquades, aquabides, whatman 42 filter paper, universal pH, chemicals from E. Merck: TEOS/Tetraethylortosilikat ( $\text{SiC}_8\text{H}_{20}\text{O}_4$ ), iron (III) nitrate nonahydrate ( $\text{Fe}(\text{NO}_3)_3 \cdot 9\text{H}_2\text{O}$ ), hydrochloric acid 37% (HCl, 37%), ethanol ( $\text{C}_2\text{H}_5\text{OH}$ ), sodium hydroxide (NaOH), ammonia, methanol ( $\text{CH}_3\text{OH}$ ), lauric acid ( $\text{CH}_3(\text{CH}_2)_{10}\text{COOH}$ ), n-hexane ( $\text{CH}_3(\text{CH}_2)_4\text{CH}_3$ ), sodium sulfate ( $\text{Na}_2\text{SO}_4$ ) anhydrous.

#### Instruments:

X-ray diffractometer type XRD-6000 Shimadzu, Gas Sorption Analyzer type Quantachrome (NOVA 11000), SEM type JEOL JSM-6510, TEM type JEOL series 1400, FTIR-8201 PC Shimadzu, Gas chromatography (GC) type Hewlett Packard 5890 series II.

### 2.2 Experimental Procedures

#### 2.2.1 Synthesis of sol silica

Sol silica was prepared by mixing 41.6 g TEOS, 10 mL HCl 2M, and 12 mL ethanol at room temperature for 2 h.

#### 2.2.2 Synthesis of $\text{SiO}_2\text{-Fe}_2\text{O}_3/\text{Mt-K10}$ nanocomposite

$\text{SiO}_2\text{-Fe}_2\text{O}_3/\text{Mt-K10}$  nanocomposite was synthesized through the intercalation process along with the calcination assisted by microwave radiation. Sol solution (Procedure 2.2.1) was mixed with 0.25 mol/L  $\text{Fe}(\text{NO}_3)_3 \cdot 9\text{H}_2\text{O}$  with the molar ratio of  $\text{Si}/\text{Fe} = 10/1$ , adopted from Han *et al.*<sup>6</sup>. The mixture was titrated with a 0.2 mol/L NaOH solution until the pH maintained at about 2.7, and then mixed with the Mt-K10 dispersion 1% w/v (CEC = 43.60 meq/100 g) at a molar ratio  $\text{Si}/\text{Fe}/\text{CEC} = 50/5/1$ . The mixture was allowed to stand for 3 h under stirring at temperature 60°C. The product was centrifuged and followed by washing with ethanol/water (1:1 volume ratio) and then dried at room temperature. The dried sample was subjected to microwave radiation power 700 W. The product was encoded as SFMK-700 and used as catalytic material.

#### 2.2.3 Characterization

The XRD patterns were obtained with a XRD-6000 diffractometer (Shimadzu) using CuK $\alpha$  radiation. IR spectra were registered with a Shimadzu PC8201 FTIR spectrophotometer. The specific surface area, pore volume, pore size distribution, and the adsorption-desorption isotherm were determined using a gas sorption analyzer (Quantachrome, NOVA 11000). The measurements were carried out at 77.4 K. TEM observation was performed with a TEM JEOL-1400 microscopy. SEM images were obtained with a SEM JEOL JSM-6510.

Total surface acidity of solids was conducted by ammonium adsorption followed by FTIR measurements. Total acidity of the samples was measured using gravimetric method.

#### 2.2.4 Catalytic activity.

The catalytic activity of the nanocomposite SFMK-700 and Mt-K10 were initiated for the lauric acid esterification in the presence of 20% (w/w) of catalyst dosage upon refluxing for 12 h of methanol and acid mixed in a molar ratio of 20:1. The final mixture was then analyzed by Gas Chromatography (GC) type Hewlett Packard 5890 series II with an FID detector. Catalyst was reactivated and then reused for two cycles of the same esterification reaction.

### 3. Results and Discussions

#### 3.1 Modification of Mt-K10 with mixedoxide SiO<sub>2</sub>-Fe<sub>2</sub>O<sub>3</sub>

The modification of montmorillonite with mixed oxide SiO<sub>2</sub>-Fe<sub>2</sub>O<sub>3</sub> was involved the intercalation of sol SiO<sub>2</sub>-Fe<sub>x</sub>(OH)<sub>y</sub> as a positive colloidal particles into the interlayer of silicate montmorillonite. Synthesis of nanocomposite Mt-K10 which is modified with SiO<sub>2</sub>-Fe<sub>2</sub>O<sub>3</sub> was started with making pillaring agent in the form of a mixture of compounds tetraortosilan (TEOS), ethanol, and HCl. TEOS hydrolyzed with acid catalyst, HCl, to form a silanol (Si-OH). This process releases the ethanol in the solution. Sol formed reacted with Fe<sup>3+</sup> ion solution and titrated with NaOH to form pillaring agent cations. Formation reaction of pillaring agent is as follows:



#### Pillaring agent

Pillaring agent [HO-Fe-O-Si(OH)<sub>2</sub>]<sup>2+</sup> subsequently undergo a process of intercalation into the montmorillonite interlayer when mixed with montmorillonite suspension. Intercalated colloidal particles which would replace the hydrated cations on montmorillonite interlayer. Montmorillonite intercalation product washed several times with a mixture of ethanol-distilled water with a ratio of 1:1 to remove residual sol. The next process was the calcination through the assistance of microwave radiation with a radiation power of 700 W to form a mixture of oxides SiO<sub>2</sub>-Fe<sub>2</sub>O<sub>3</sub> in the interlayer Mt-K10.

#### 3.2 Characterization of chemicals and physical properties of nanocomposite

The initial characterization of Mt-K10 was carried out without washing or other treatment. The same characterization was continued for nanocomposite (SFMK-700).

Fig. 1 shows the series of XRD patterns of Mt-K10 and SFMK-700.

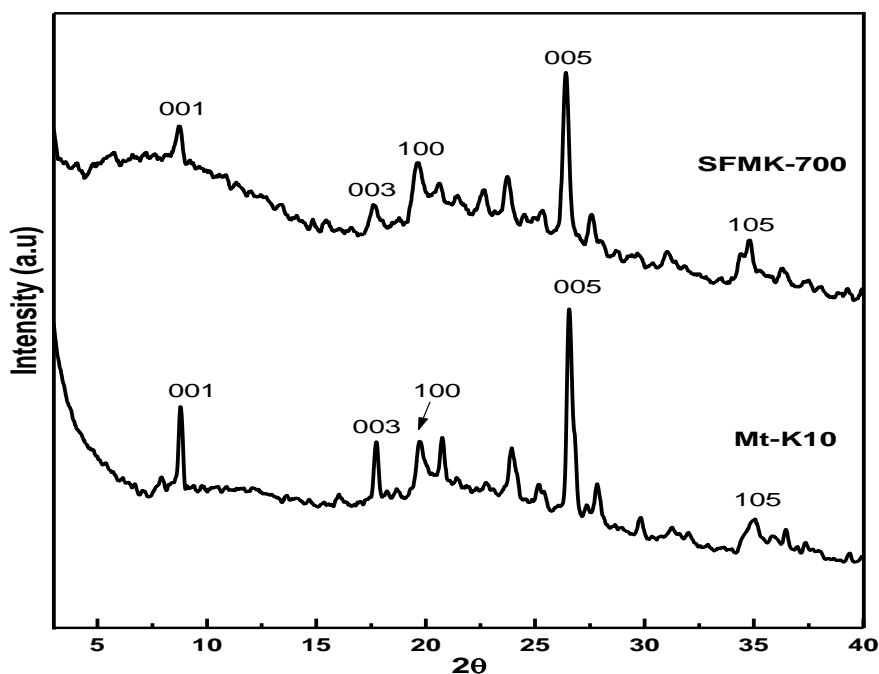
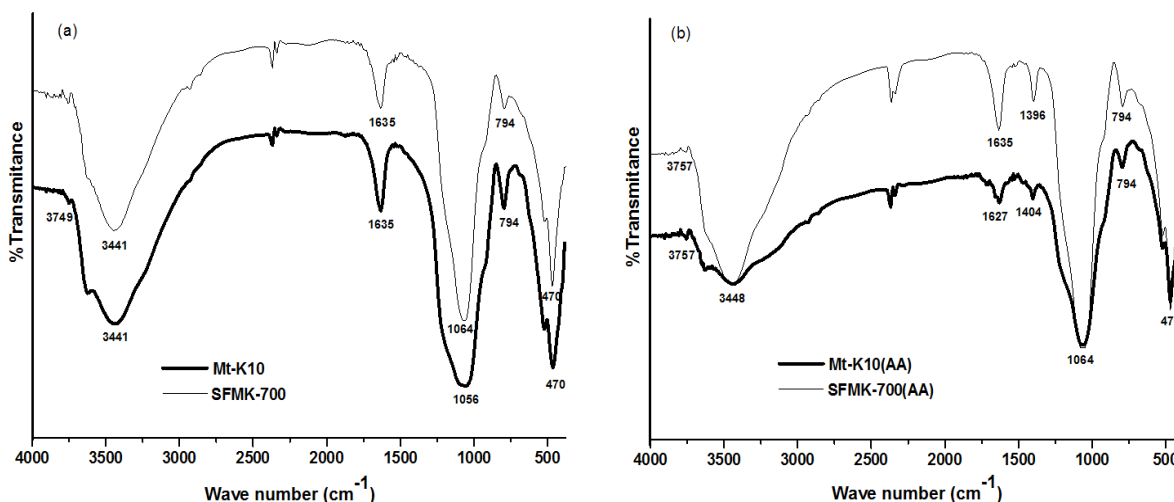


Fig. 1 Diffraction patterns of (a) Mt-K10 and (b) SFMK-700

In general, the XRD patterns of modified montmorillonite (Fig. 1(b)) assisted by microwave radiation virtually unchanged compared to the Mt-K10 (Fig. 1(a)). Mt-K10 shows diffraction peaks at 8.79° (001), 17.71° (003), 19.72° (100), 26.56° (005), and 34.89° (105) corresponding to montmorillonite of hexagonal phase. These diffraction peaks are similar to that reported by Kumar *et al.*<sup>7</sup> and Ghebauret *al.*<sup>8</sup>. The 001 reflection at

8.79° ( $d=1.005$  nm) of Mt-K10 was shifting to the lower angle 8,68° and slightly increased to  $d=1,017$ nm (SFMK-700). This is indicating that upon calcination at 700 W,  $\text{SiO}_2\text{-Fe}_2\text{O}_3$  nanosol transform into mixed oxides in the interlayer Mt-K10, also as particles on the surface of Mt-K10 (Fig.4).



**Fig. 2 FTIR Spectra of Mt-K10 and SFMK-700 (a) before and (b) after adsorbed ammonia**

Fig. 2(a) shows the important bands for identification of montmorillonite and nanocomposite SFMK-700. The absorption band at  $3441$  and  $3749\text{cm}^{-1}$  are identified as structural  $\text{-OH}$  stretching vibration of water molecules and  $\text{-OH}$  stretching vibration of structural octahedral  $\text{Al-OH}$ . Those bands are reinforced with bending vibration bands of  $\text{-OH}$  water molecules at  $1635\text{cm}^{-1}$ . This is an indication that montmorillonite has a water absorbing properties<sup>9</sup>. Stretching and bending vibration of water molecules became weak and have medium intensity for the SFMK-700 nanocomposite. This is due to dehydration and dehydroxylation experienced during thermal agitation when the microwave radiation process takes place. Molu and Yurdakoç<sup>10</sup> reported that pillaring process replaces a large amount of hydrated interlayer cations and it decreased absorption band intensity.

Absorption band at  $470\text{cm}^{-1}$  is characteristic of bending vibration of  $\text{Si-O-Si}$ , while band at  $1056\text{cm}^{-1}$  is a characteristic of stretching vibration of  $\text{Si-O}$  in the tetrahedral. It was shifted to higher wave number  $1064\text{cm}^{-1}$  with the increasing in the intensity due to strong  $\text{Si-O}$  bond. This is an indication of the strength of the bond between the silicate layers of montmorillonite with  $\text{SiO}_2\text{-Fe}_2\text{O}_3$ . The band at  $794\text{cm}^{-1}$  is due to stretching vibration of  $\text{Al}_{\text{IV}}$  tetrahedral, the intensity decreased due to dealumination after the calcination process.

The characteristic of Brønsted acidity was showed by intense peak at  $1404\text{cm}^{-1}$  and  $1396\text{cm}^{-1}$  for Mt-K10 and SFMK-700, respectively (Fig. 2(b)). This peak does not appear on the samples prior to absorb ammonia (Fig. 2(a)). Qualitatively, acid sites strength can be seen from the absorption peaks in the wavelength range that shows the interaction between the catalyst and the ammonia.  $\text{NH}_3$  adsorption on Mt-K10 and SFMK-700 samples leads to formation of strongly bound coordinated ammonia, which is evidenced strong Brønsted acidity. According to Emeis<sup>11</sup>, the number of Brønsted or Lewis acid is proportional to band area of the Brønsted or Lewis peak. A specific area of the peak that indicates the acidity Brønsted is equal to  $1.15$  and  $1.92$  for the Mt-K10 and SFMK-700, respectively. Thus, the catalyst SFMK-700 has a lot more acidic sites than Mt-K10. This occurs due to the presence of a mixture of metal oxides of  $\text{Si-Fe}$  in the Mt-K10 interlayer which contributed to the acid sites. This data are also reinforced by the results of total acidity. The total acidity increased by  $4.93\text{mmol/g}$  for the SFMK-700 catalyst, while the Mt-K10 is  $4.83\text{mmol/g}$ .

Table 1 shows the nitrogen gas adsorption analysis data, while the Fig. 3 shows the adsorption-desorption isotherm of nitrogen and pore size distribution.

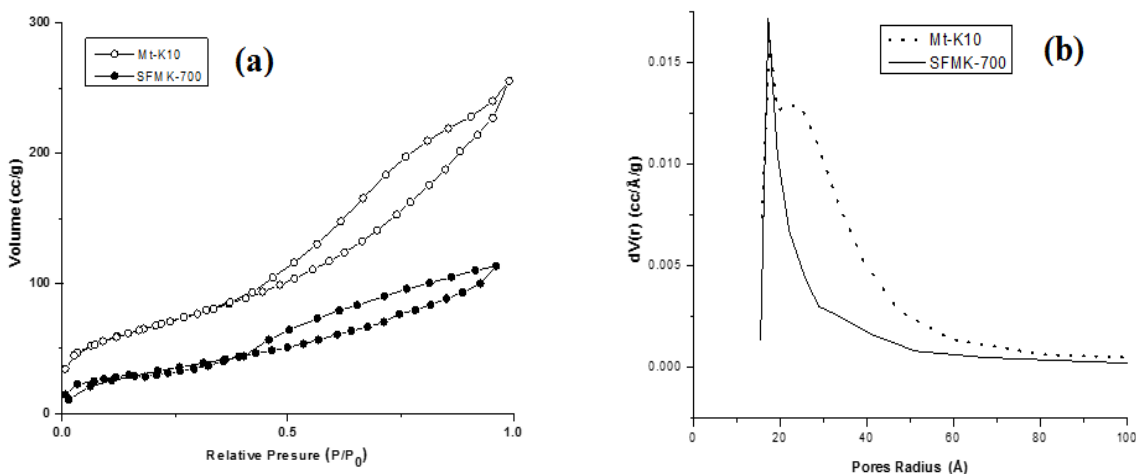
**Table 1. Nitrogen adsorption analysis**

Sample	Surface area <sup>a</sup> (m <sup>2</sup> g <sup>-1</sup> )	Total pore volume <sup>b</sup> (cm <sup>3</sup> g <sup>-1</sup> )	Average pore radius <sup>b</sup> (Å)
Mt-K10	240,0	0,3950	32,92
SFMK-700	105,6	0,1754	33,23

<sup>a</sup>determined by the multipoint BET method

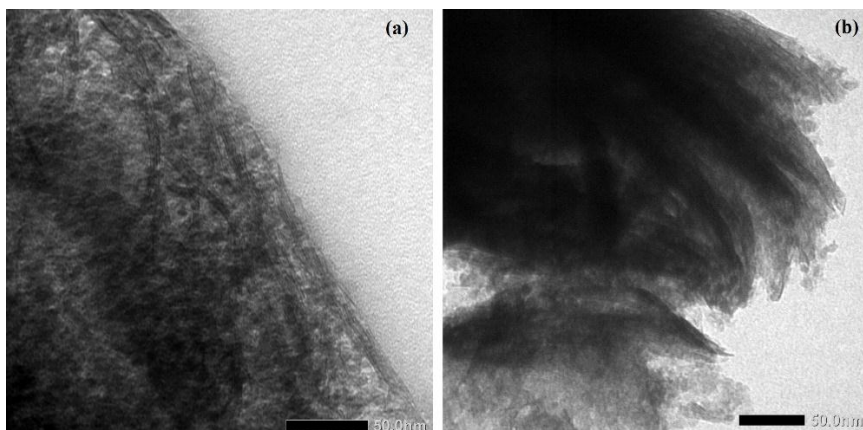
<sup>b</sup>determined using BJH pore analysis.

The decreased of surface area and total pore volume of nanocomposite SFMK-700 were caused by contributed of the SiO<sub>2</sub>-Fe<sub>2</sub>O<sub>3</sub> particles on the surface of montmorillonite that cover the pores or even the interlayer of Mt-K10 during the calcination process takes place This can be evidenced by the data TEM micrographs (Fig. 4(b)). Some literature reported a decrease in the surface area of montmorillonite caused by the deposit of iron oxide particles, Fe<sub>2</sub>O<sub>3</sub>, on the surface of solids<sup>7,12</sup>.

**Fig.3(a) Adsorption-desorption isotherm of nitrogen and (b) pore size distribution**

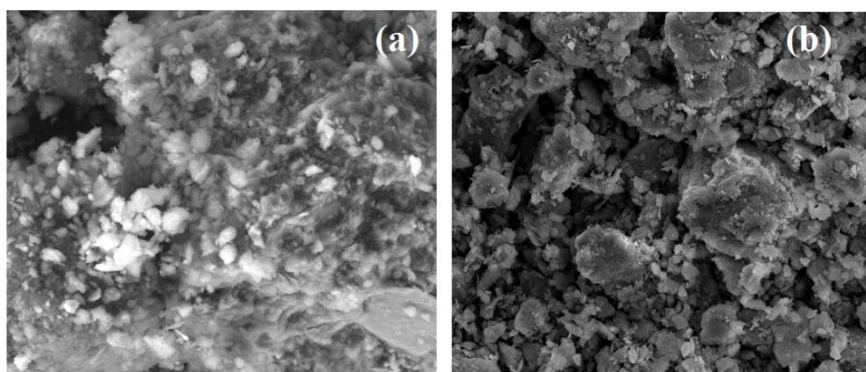
The nitrogen adsorption-desorption isotherm of Mt-K10 and SFMK-700 are presented in Fig.3(a). The isotherms of all samples were similar and almost had the same shape. They corresponded to type IV according to BDDT classification<sup>13</sup>, where most of the nitrogen is adsorbed in mesopores of the nanocomposite materials, and their hysteresis loops are of type H3 according to the IUPAC classification, indicating the presence of slit-shape pore<sup>14</sup>. Adsorption of non-polar gases by montmorillonite clays and the aggregates of other platy particles typically given the type H3 of the hysteresis loop, as reported literally<sup>15,16</sup>. This experiment clearly demonstrated that the nitrogen uptake decrease continuously due to the small surface area of the nanocomposite.

Fig. 4(b) shows the pattern of the pore size distribution of the samples calculated by BJH method. The pore size distribution of SFMK-700 is slightly different to that described for Mt-K10. It might be due to an increasing in the proportion of macropores when Si-Fe is added to the system. The SFMK-700 has a narrow size distribution and exhibits a population of mesopores.



**Fig. 4 TEM Micrograph of (a) Mt-K10 and (b) SFMK-700**

TEM micrographs (Fig. 4) showing the morphology of multilayer silicate Mt-K10 more regular after the intercalation process by mixed metal oxide  $\text{SiO}_2\text{-Fe}_2\text{O}_3$  using microwave radiation (Fig. 4(b)). This indicates that the two phases of the pillars and the Mt-K10 silicate layers bonded well. There are some mixed oxides  $\text{SiO}_2\text{-Fe}_2\text{O}_3$  permanently connecting montmorillonite sheet silicate. Mt-K10 has the delaminate or exfoliated structure, while SFMK-700 has the intercalated nanocomposite structure. According to Alexandre and Dubois<sup>16</sup>, intercalated nanocomposites obtained if at least one polymer chain intercalated between the silicate layers produces multilayer morphology. The existence of mixed oxides  $\text{SiO}_2\text{-Fe}_2\text{O}_3$  on silicate interlayer even on the surface of montmorillonite nanocomposite indicated by black spots.



**Fig.5 Image SEM of (a) Mt-K10 (left) and (b) SFMK-700 (Magnification 2000x)**

SEM image of Mt-K10 and SFMK-700 shown in Figure 5. Both images showed the typical morphology of porous material which is irregular and rough. A similar case was reported by Muthuve *et al.*<sup>12</sup> when encapsulates Fe on montmorillonite. Aggregate particles of SFMK-700 nanocomposite showed the darker particles due to the presence of Si-Fe oxides mixture.

### 3.2 Catalytic activity for methyl ester synthesis

Catalytic activity test carried out on esterification of lauric acid with methanol using catalysts Mt-K10 and SFMK-700. For comparison purposes, experiment was also carried out without using a catalyst (blank reaction). The conversion of lauric acid into methyl laurate on pure and pillared Mt-K10 catalysts has been investigated by GC. Total conversion and product yield, determined based on a chromatogram of reaction, were calculated using eqs. (1) and (2).

$$\text{Total conversion (\%)} = \frac{[\text{Lauric acid}]_0 - [\text{Lauric acid}]_f}{[\text{Lauric acid}]_0} \times 100 \quad (1)$$

$$\text{Methyl laurate yield (\%)} = \frac{\% [\text{Methyl laurate}] \times \text{Weight of product}}{\text{Weight of lauric acid}} \times 100 \quad (2)$$

Here,  $[\text{Lauric acid}]_0$  and  $[\text{Lauric acid}]_f$  are the concentrations of lauric acid in unreacted and in the product. Weight of lauric acid is initial weight as a reactant. The data are presented in Fig. 6:

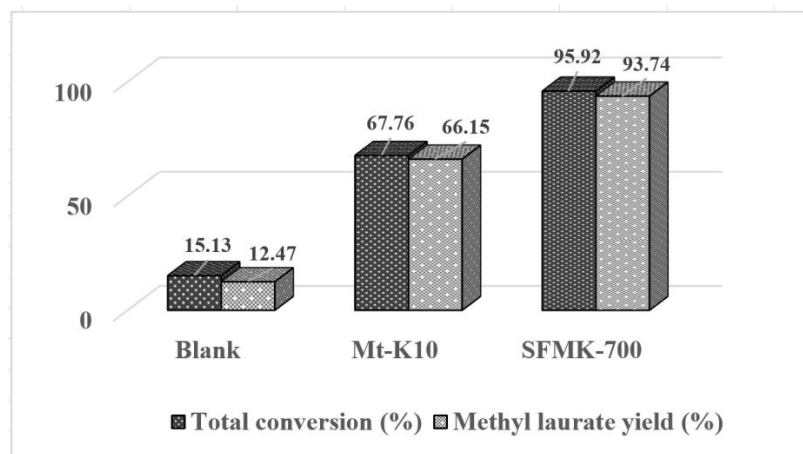


**Fig. 6 Histogram total conversion and methyl laurate yield**

By observing the conversions of lauric acid to methyl laurate (Fig. 6), it is apparent that all materials have catalytic activity under the conditions applied in this study. Similar behaviour was reported by Zatta *et al.*<sup>18</sup> when developing phosphoric acid activated clays. In their case, there seemed to be a limit in acid concentration and time of treatment to develop the best catalyst for the esterification of lauric acid with methanol. Evident from our results that catalyzed esterification reaction proved very large conversion and product yields compared to the reaction without a catalyst. While the esterification reaction with pillared Mt-K10 catalyst with a mixture of Si-Fe metal oxide calcined by microwave radiation provides higher results than the host material, Mt-K10.

Nanocomposite SFMK-700 has a smaller polarity due to the inclusion of the mixed metal oxide in the interlayer Mt-K10 (physical observations by solubility in water). Thus the hydrophobicity of the nanocomposite will increase. Consequently in reaction, methanol will minimize interactions with the pore walls of solids SFMK-700, so that the rate of diffusion to the active sites will be faster. This allows the esterification reaction to run faster.

This experiment did not study the mechanisms of the esterification by solid acid catalysts, but it seems to follow the reaction step of methyl ester formation through the esterification reaction using solid acid catalysts as proposed by Di Serio *et al.*<sup>19</sup>. Carbonyl group of lauric acid adsorbs on Lewis acid site and methanol adsorbs on the basic site of the catalyst to produce carbocation (step 1). Then, at the surface of the catalyst (step 2), nucleophilic attack of carbocation at each methanol hydroxyl group. The nucleophilic attack would generate tetrahedral intermediate. Finally (Step 3), the product methyl laurate was formed from desorption of hydroxyl group from catalyst surface after breaking the -OH bond while the deprotonated catalyst regenerated the active species for starting another catalytic cycle. H<sub>2</sub>O was formed as a product of the esterification after the catalytic cycle was completed.

### 3.3 Catalyst recovery and reusability

The final stage is the recovery and reuse of the catalyst for two cycles of the same reaction. The catalyst is separated, washed with n-hexane, dried at room temperature and is activated by microwave radiation of 200 W for 10 minutes. Figure 7 shows a decrease in activity of the catalyst for the next cycle. This is caused by decrease of Lewis or Brønsted acid sites due to the washing process or other stages of the esterification reaction is undertaken.

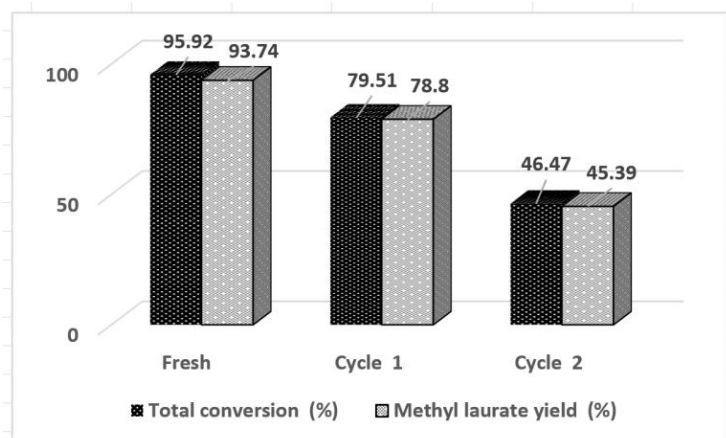


**Fig. 7 Histogram of reusecatalyst**

Reduction in catalyst activity in the second cycle is very large. This is because the released of iron species from the active site surface of montmorillonite.

#### 4. Conclusion

This research proves that the modification of montmorillonite K10 with mixed oxide  $\text{SiO}_2\text{-Fe}_2\text{O}_3$  resulting in increased of the acidity and catalytic activity of the nanocomposite. A high conversion of lauric acid to methyl laurate as much as 93.74%, which proves that the catalyst can be used for methyl ester (biodiesel) synthesis.

#### Acknowledgement

The authors are grateful to Kemenristek dikti Indonesia for financial assistances through Doctoral Dissertation Grant 2016, number:44/UN13.3/SPK-PJ/LP-HB/2016.

#### References

1. Fazaeli, R., Aliyan, H., 2007, Clay (KSF and K10)-supported heteropoly acids: Friendly, efficient, reusable and heterogeneous catalysts for high yield synthesis of 1,5-benzodiazepine derivatives both in solution and under solvent-free conditions, *Appl. Catal. A: General* 331, pp. 78–83.
2. Aher, R. D., Gade, M.H., Reddy, R.S., Sudalai, A., 2012,  $\text{Cu}^{\text{II}}$ -exchange montmorillonite K10 clay-catalyzed direct carboxylation of terminal alkynes with carbon dioxide, *Indian J. Chem.*, Vol.51A, pp. 1325-1329.
3. Arunkumar, R., Subramani, K., Ravichandran, S., 2010, Montmorillonite K10 clay catalyzed microwave synthesis of some Mannich bases and their characterization, *Int. J. ChemTech. Res.*, Vol. 2, No.1, pp. 278-281.
4. Ayoub, M., Abdullah, A.Z., 2013, Short Communication: LiOH-modified montmorillonite K-10 as catalyst for selective glycerol etherification to diglycerol, *Catal. Commun.* 34, pp. 22–25.
5. Sekewael, S.J., Wijaya, K., Triyono, Budiman, A., 2016, Microwave assisted preparation and physico-chemical properties of mixed oxides silica-zirconia montmorillonite K10 nanocomposite, *Asian J. Chem.*, 28 No.10, pp. 2325-2330.
6. Han, Y.S., Matsumoto, H., and Yamanaka, S., 1997, Preparation of new silica sol-based pillared clays with high surface area and high thermal stability, *Chem.Mater.* 9, 2013-2018.
7. Kumar, J.P., Ramacharyulu, P.V.R.K., Prasad, G.K., and Singh, B., 2015, Montmorillonites supported with metal oxide nanoparticles for decontamination of sulfur mustard, *Appl. Clay Sci.*, 116-117, pp. 263-272 (2015).
8. Ghebaour, A., Gârea, S. A., Iovu H., 2011, The influence of inorganic host type in the drug-layered silicate biosystems, *U.P.B. Sci. Bull.*, Series B, Vol. 73, Iss. 3, pp.169-176.

9. Utubira, Y., Wijaya, K., Triyono, Kunarti, E. S., 2016, Microwave assisted preparation of zirconia-pillared bentonite, *Int. J. ChemTech. Res.*, Vol. 9., No. 4., 475-482.
10. Molu, Z. B., Yurdakoç, K., Preparation and characterization of aluminum pillared K10 and KSF for adsorption of trimethoprim, *MicroporousMesoporous Mater.* 127, 50–60 (2010).
11. Emeis, C.A., 1993, Determination of integrated molar extinction coefficient for infrared absorption of pyridine adsorbed on solid acid catalyst, *J. Catal.*, Vol. 141, Iss. 2. 347-354. doi: 10.1006/jcat.1993.1145.
12. Muthuvel, I., Krishnakumar, B., Swaminathan, M., 2012, Novel Fe encapsulated montmorillonit K10 clay for photo-Fenton mineralization of Acid Yellow 17, *Indian J. Chem.*, vol 15, 800-806.
13. Gregg, S.J. and Sing, K.S.W., *Adsorption, Surface Area and Porosity*, Academic Press, London. (1982).
14. Yuan, P., Bergaya, F.A., Tao, Q., Fan, M., Liu, Z., Zhu, J., He, H., and Tianhu Chen, 2008, A combined study by XRD, FTIR, TG and HRTEM on the structure of delaminated Fe-intercalated/pillared clay, *J. Colloid Interface Sci.* 324: 142-149.
15. Barrer, R.M., Clay minerals as selective and shape-selective sorbents, *Pure & Appl. Chem.*, Vol. 61, No.11, 1903-1912 (1989).
16. Sing, K. S.W. and Williams, R.T, Pysisorption Hysteresis loop and the characterization of nanoporous material, Review, *AST*, 22 (10)\_64, 773-782 (2005).
17. Alexandre, M., Dubois, P., Polymer-layered silicate nanocomposites: preparation, properties and uses of a new class of materials, *Mater. Sci. Eng.* 28, 1-63 (2000).
18. Zatta, L., Ramos, L.P., Wypych, F., 2013, Acid-activated montmorillonites as heterogeneous catalysts for the esterification of lauric acid acid with methanol, *Appl. Clay Sci.* 80–81, 236–244.
19. Di Serio, M., Tesser, R., Pengmei, L., and Santacesaria, E., 2008, Heterogeneous catalysts for biodiesel production, *Energy Fuels*, 22,207–217.

\*\*\*\*\*